Int. J. Multiphase Flow Vol. 10, No. 1, pp. 41–60, 1984
Printed in Great Britain.

0301-9322/84 $3.00 + .00
Pergamon/Elsevier

A THEORETICAL MODEL FOR CORE-ANNULAR FLOW OF A VERY VISCOUS OIL CORE AND A WATER ANNULUS THROUGH A HORIZONTAL PIPE

G. OOMS,† A. SEGAL and A. J. VAN DER WEES‡
Delft University of Technology, Delft, The Netherlands

and

R. MEERHOFF and R. V. A. OLIEMANS
Koninklijke/Shell-Laboratorium Amsterdam, Amsterdam, The Netherlands

(*Received* 19 *October* 1982; *in revised form* 16 *May* 1983)

Abstract—A theoretical model has been developed for core-annular flow of a very viscous oil core and a water annulus through a horizontal pipe. Special attention was paid to understanding how the buoyancy force on the core, resulting from any density difference between the oil and water, is counterbalanced. This problem was simplified by assuming the oil viscosity to be so high that any flow inside the core may be neglected and hence that there is no variation of the profile of the oil–water interface with time. In the model the core is assumed to be solid and the interface to be a solid/liquid interface.

By means of the hydrodynamic lubrication theory it has been shown that the ripples on the interface moving with respect to the pipe wall can generate pressure variations in the annular layer. These result in a force acting perpendicularly on the core, which can counterbalance the buoyancy effect.

To check the validity of the model, oil–water core-annular flow experiments have been carried out in a 5.08 cm and an 20.32-cm pipeline. Pressure drops measured have been compared with those calculated with the aid of the model. The agreement is satisfactory.

1. INTRODUCTION

Pipeline transport of a very viscous oil can be effected by heating the oil and insulating the pipeline. However, these operations involve considerable capital investment and operating expenditure.

Another possibility is the simultaneous transport through the pipe of the highly viscous oil and an immiscible "low-viscosity" liquid such as water. In the past, experiments have been carried out to examine this possibility; see for instance Charles *et al.* (1961). During these experiments a number of different flow patterns were observed, such as water drops in oil, concentric oil-in-water (core-annular flow), oil slugs in water and oil drops in water. The pressure drops measured over the pipe indicated that the addition of water greatly reduced the pressure gradient.

It was found that of all the observed flow patterns the flow of the highly viscous oil as a core, with the water flowing only in the annular space between the core and the pipe wall, was the most desirable for simultaneous flow. The experiments showed that in the case of core-annular flow the pressure drop over the pipe could be of the same order of magnitude as, or even smaller than, the pressure drop for the flow of water alone at the same mean velocity as for the mixture. The annular film can be very thin and thus the amount of water required small, so that the pumping power necessary to move this water is negligible. The mode of core-annular flow also has the advantage that the contact surface area between oil and water is minimal. Entrainment of one liquid by the other may be expected to be much less than with the other flow patterns.

†Laboratory of Aerodynamics and Hydrodynamics
‡Mathematics Department

One of the central questions regarding core-annular flow in a horizontal pipe is how the buoyancy force on the core, resulting from any density difference between oil and water, is counterbalanced. In this paper a theoretical model is developed which gives a possible answer to this question. In this model the oil viscosity is assumed to be so high that any flow in the core, and hence any variation in the oil–water interface form with time, may be neglected. So the core is assumed to be solid and the interface to be a solid/liquid interface.

The core surface is assumed to be rippled, on the basis of observations during the experiments. The simplification to a solid core permits free choice of the wavelength and shape of the ripple. However, in order to make this choice as realistic as possible, experiments were carried out to determine the shape of the ripple.

In order to check the validity of the model oil–water core-annular flow pressure drop measurements were also made in 5.08 cm and an 20.32 cm pipeline. These measurements have been compared with pressure drops predicted with the aid of the model.

2. EXPERIMENTAL INVESTIGATION OF RIPPLE SHAPE

The experiments were performed in a perspex pipe 50 m long and 0.05 m in diameter. The difference in density between water and the oil was about 30 kg/m^3. The amount of water was varied between 20% and 1%. Oil and water were introduced into the pipe via an inlet device, which consisted of a central tube surrounded by an annular slit. The oil was supplied via the tube, the water via the slit.

Although the oil core was pumped into the pipe concentrically, it adjusted itself eccentrically, due to the density difference. As long as the oil core was supplied at a velocity above a certain critical value (~ 0.1 m/s), a water film remained between the oil core and the pipe wall, not only in the lower part of the pipe, but also in the upper part. However, in the upper part the film was much thinner. Some photographs of the experiments are shown in figures 1(a)–(c). In the figures the flow is from left to right. The section shown is located 1 m from the bend downstream of the inlet device. Only when the oil core was supplied at a velocity below the cirtical value did it touch and foul the upper part of the pipe. In that case the flow pattern changed from eccentric core-annular to stratified, with all the oil in the upper part of the pipe and the water only in the lower part.

Above the critical velocity the eccentric core-annular flow was steady after a few diameters. Changing the amount of water did not affect the flow pattern very much; the thin water film in the upper part remained almost the same, only the thickness of the water film in the lower part changing (see figures 1 a–c). The observations also indicated that in the upper part the thickness of the water film is nearly independent of the tangential coordinate; in the lower part the thickness increases towards the bottom of the pipe. For the computational modelling it was, therefore, assumed that the thickness of the water film in the upper part is constant; in the lower part it increases linearly with θ (see figure 2). During some of the experiments a rectangular roughness element was placed against the pipe wall at a certain location inside the pipe in order to study the reaction of the flow to such a disturbance. The eccentric core-annular flow passed this disturbance without difficulty; a few diameters downstream it was steady again.

Immediately after the inlet device a ripple appeared at the oil-water interface. The rate of growth of the amplitude of this ripple was quickly damped out; so a ripple with a finite amplitude remained at the interface. At the top of the core the ripples have a sawtooth-like shape. The wavelength is of the same order of magnitude as the radius of the pipe. From the observations it could not be concluded that the bottom ripples are similar to the top ripples. In some cases the photographs even suggest possible opposite asymmetries at top and bottom. However, as will be shown later, the important part of the water film is at the top, where the downthrust due to lubrication forces is generated. The lubrication forces at the bottom are negligible. To facilitate the computational modelling it is, therefore, permissible to assume in

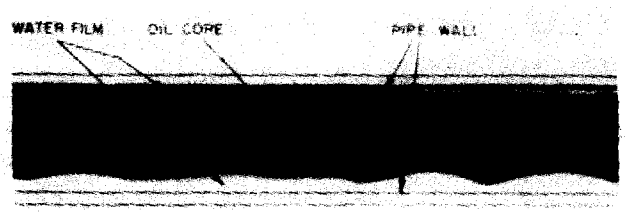

(a) 11.1% WATER

(b) 8% WATER

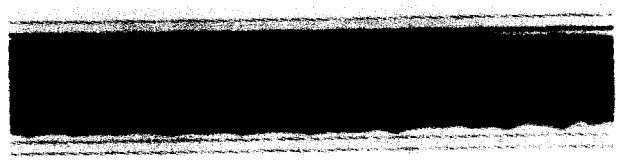

(c) 6.3% WATER

Figure 1. Experiments with oil–water core-annular flow in a 2-inch pipe. The flow is from left to right.

the calculations that the bottom ripples are similar to the top ripples. So the ripple shape is assumed to be independent of θ (see figure 2).

3. THEORETICAL MODEL

As mentioned in the introduction, the oil core is assumed to be solid and hence the oil–water interface to be a solid/liquid interface. The reason for this assumption is that it simplifies the

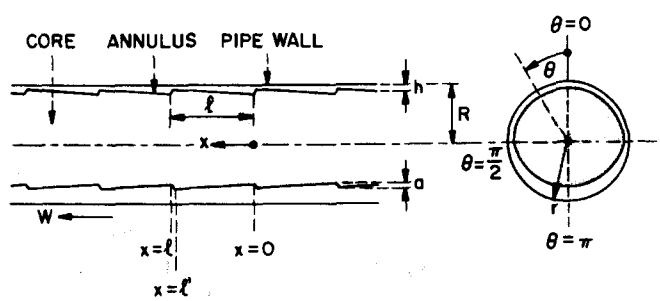

Figure 2. Core-annular flow with a sawtooth-shaped solid core.

flow problem considerably. To solve the real flow problem, in which both core and annulus have a finite viscosity, is very difficult.

A frame of reference is chosen, according to which the core is at rest and the pipe wall has a velocity W in the x-direction (see figure 2). r, θ and x are cylindrical coordinates. $h(\theta, x)$ represents the thickness of the water annulus and R is the radius of the pipe. In accordance with the observations, the solid core is assumed to be rippled. In the x-direction (θ = constant) h is assumed to be periodic and of sawtooth shape; the wavelength l is of the same order of magnitude as R. As explained in paragraph 2 the ripple shape is assumed to be independent of θ. In the θ-direction (x-constant) h is assumed to be symmetric with respect to the line through $\theta = 0$ and $\theta = \pi$ (see figure 2). As also explained in paragraph 2 for $0 \leqslant \theta \leqslant \pi/2$, h is assumed to be independent of θ; for $\pi/2 < \theta \leqslant \pi$ h increases linearly with θ (see figure 2). This can be written as

$$h = h_0 - e - a\frac{x}{l'} \text{ for } 0 \leqslant \theta \leqslant \pi/2 \text{ and } 0 \leqslant x \leqslant l' \qquad [1]$$

$$h = h_0 - e - a + a\frac{(x - l')}{(l - l')} \text{ for } 0 \leqslant \theta \leqslant \pi/2 \text{ and } l' \leqslant x \leqslant l \qquad [2]$$

$$h = h_0 - e - a\frac{x}{l'} + 4e\frac{(\theta - \pi/2)}{\pi/2} \text{ for } \pi/2 \leqslant \theta \leqslant \pi \text{ and } 0 \leqslant x \leqslant l' \qquad [3]$$

$$h = h_0 - e - a + a\frac{(x - l')}{(l - l')} + 4e\frac{(\theta - \pi/2)}{\pi/2} \text{ for } \pi/2 < \theta \leqslant \pi \text{ and } l' < x \leqslant l. \qquad [4]$$

At the trough of the ripple ($x = 0$) the film thickness is $h_0 - e$ at the top and $h_0 + 3e$ at the bottom, where e represents half the eccentricity of the core. The parameter a gives the amplitude of the ripple in the core surface (see also figure 2). At the trough the surface area of the water film in the upper part of the pipe is equal to $2 \cdot (\pi/2)\, R \cdot (h_0 - e)$, and in the lower part $2\{(\pi/2)\, R \cdot (h_0 - e) + (1/2) \cdot (\pi/2)\, R \cdot 4e\}$. So the total area of the water film is $2\pi R h_0$, and the mean thickness of the water film at the trough is given by h_0. l' is the distance from $x = 0$ to the minimum in h.

The purpose of the calculation below is to investigate the nature of steady, eccentric core-annular flow. For a steady situation to arise a balance is required between the buoyancy force on the core and the vertical components of the pressure forces and viscous forces on the core generated by the water flow in the annulus. In the calculation the hydrodynamic lubrication theory will be applied to the water flow in the annulus. This means that the following conditions are assumed to hold

$$\frac{a}{R} \ll 1 \qquad [5]$$

$$\frac{a}{l} \ll 1 \qquad [6]$$

$$\frac{\rho W h}{\mu} \cdot \frac{a}{l} \ll 1, \qquad [7]$$

in which ρ represents the density of the water in the annulus and μ the viscosity of water.

From the visual observations discussed in section 2 it can be concluded that the conditions [5] and [6] are satisfied. To calculate condition [7] the values of h, a and l have to be known. From the observations it can be concluded that due to the buoyancy effect the water film is extremely thin in the upper part of the pipe. It is, however, very difficult to perform

accurate measurements of h and a in the upper part. As mentioned earlier, the important part of the water film is at the top, where the downthrust due to lubrication forces is generated. The lubrication forces at the bottom are negligible. In the coming calculation it is, therefore, assumed that condition [7] is also satisfied. It will obviously have to be checked in due course whether the results of calculations made with the model indeed satisfy condition [7].

At the moment it is not known how the ripple height and wavelength should be selected from known properties and velocities of the fluids. The present calculation was therefore based on the photographs taken during the tests in the 2-inch pipe (see figure 1) and the pressure losses measured. In order to improve the prediction of the ripple parameters the authors of this paper are developing a new calculation method. It is an extension of the method given by Yih (1967) for the calculation of the stability of plane Couette–Poiseuille flow of two superposed layers of liquids of different viscosity. Yih showed that such a flow can be unstable, however small the Reynolds number is. Wondering what would happen to the flow when it was unstable and slightly disturbed, Yih came to the conclusion that stable waves of finite amplitude would occur at the interface. In addition, experiments are planned in which the ripple height and wavelength will be measured as a function of the fluid properties and velocities. The experimental results will be compared with theoretical predictions. The authors hope to report on this experimental and theoretical work in the near future.

The starting-point of the calculation is the basic equation of the hydrodymanic lubrication theory: the so-called Reynolds equation

$$\frac{\partial}{\partial\theta}\left(\frac{h^3}{R^2}\frac{\partial\phi}{\partial\theta}\right)+\frac{\partial}{\partial x}\left(h^3\frac{\partial\phi}{\partial x}\right)=6\mu W\frac{\partial h}{\partial x}. \qquad [8]$$

For the derivation of the Reynolds equation see, for instance, Tipei (1962).

The variable ϕ is given by

$$\phi = p + \rho g r\cos\theta, \qquad [9]$$

in which p is the pressure at pipe centre level and g the acceleration due to gravity. Equation [8] is solved for the water flow in the annulus. Because of symmetry (see figure 2) the boundary conditions for ϕ in the θ-direction are given by

$$\text{for } \theta = 0 : \frac{\partial\phi}{\partial\theta} = 0 \qquad [10]$$

$$\text{for } \theta = \pi : \frac{\partial\phi}{\partial\theta} = 0. \qquad [11]$$

With respect to the boundary conditions in the x-direction it is assumed that

$$\text{for } x = 0 : \phi = \phi_1 \text{ (is constant)} \qquad [12]$$

$$\text{for } x = nl : \phi = \phi_2 \text{ (is constant)} \qquad [13]$$

in which n is an integer, and $(\phi_2 - \phi_1)/nl$ is the pressure gradient over the pipe. The objective in taking a number of wavelengths n into account is to find the periodic solution. As will be shown later, $n = 7$ is sufficient for the lubrication approximation to settle to near-periodic conditions. To be on the safe side $n = 13$ is used in all the calculations.

Once the pressure ϕ is known, the velocity components of the water in the θ-direction (v) and the x-direction (w) can be calculated from the following two equations derived with the aid

of the hydrodynamic librication theory

$$v = \frac{1}{2\mu R}\frac{\partial \phi}{\partial \theta}\, y(y-h) \qquad [14]$$

$$W = \frac{1}{2\mu}\frac{\partial \phi}{\partial x}\, y(y-h) + W\left(1-\frac{y}{h}\right), \qquad [15]$$

in which y is the radial distance from the pipe wall

$$y = R - r. \qquad [16]$$

For known values of ϕ, v and w the force F_1, exerted by the water on the core in the horizontal direction and the force F_3, exerted in the downward direction, can then be calculated. The force F_i, exerted by the water on the core over a ripple wavelength l half-way between $x = 0$ and $x = nl$ in the i-direction, is given by

$$F_i = \int\int_{S_3} (p\delta_{ij} - \sigma'_{ij}) n_j^{(c)}\, dS, \qquad [17]$$

in which S_3 is the core surface between x and $x + l$ as shown in figure 3, δ_{ij} is the Kronecker symbol, σ'_{ij} the viscous stress tensor and $n_j^{(c)}$ the unit normal on the core as shown in figure 3. As the integral of [17] is difficult to calculate, F_i will be expressed in an integral over the surface S_4 of the pipe wall (see figure 3). To this end we make use of the fact that in steady flow the pressure forces and viscous forces exerted on the volume of water bounded by S_1 to S_4 must balance the weight of the water. Hence

$$\int\int_{S1} p\delta_{i1}\, dS - \int\int_{S_2} p\delta_{i1}\, dS - \int\int_{S_3} (p\delta_{ij} - \sigma'_{ij}) n_j^{(c)}\, dS - \int\int_{S_4} (p\delta_{ij} - \sigma'_{ij}) n_j^{(p)}\, dS = -\rho g V_w \delta_{i3}, \qquad [18]$$

in which the surfaces S_1 and S_2 are as indicated in figure 3, $n_j^{(p)}$ is the unit normal on the pipe wall (see figure 3) and V_w is the volume of the water bounded by S_1 to S_4. The integer 1 in δ_{i1} refers to the horizontal axis in the x-direction, and the integer 3 in δ_{i3} to the downward vertical axis. The S_1 and S_2 integrals contribute no vertical force. However, they do contribute a horizontal force due to the pressure gradient over the pipe. For this reason they are not omitted

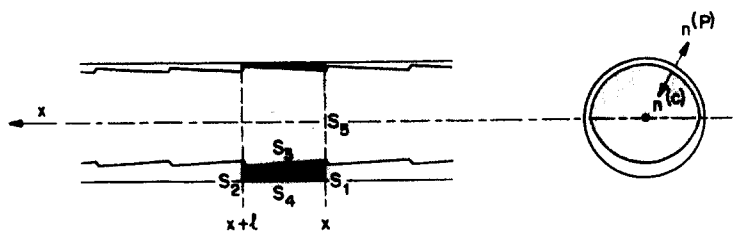

Figure 3. Control volume in the annulus bounded by the surfaces S_1–S_4.

in [18]. Substitution of [18] in [17] gives

$$F_i = \iint_{S_1} p\delta_{i1}\,dS - \iint_{S_2} p\delta_{i1}\,dS - \iint_{S_4} (p\delta_{ij} - \sigma'_{ij})\,n_j^{(p)}\,dS + \rho g V_w \delta_{i3}. \qquad [19]$$

For the downward vertical direction ($i = 3$) [19] becomes, after substitution for σ'_{ij}

$$F_3 = 2R\int_0^{\pi}\int_0^{l} (p)_{y=0}\cos\theta\,d\theta\,dx + 2\mu R\int_0^{\pi}\int_0^{l}\left(\frac{\partial v}{\partial y}\right)_{y=0}\sin\theta\,d\theta\,dx + \rho g V_w. \qquad [20]$$

In steady flow the force F_3 exerted by the water on the core must balance the gravity force on the core. Hence,

$$2R\int_0^{\pi}\int_0^{l} (p)_{y=0}\cos\theta\,d\theta\,dx + 2\mu R\int_0^{\pi}\int_0^{l}\left(\frac{\partial v}{\partial y}\right)_{y=0}\sin\theta\,d\theta\,dx + \rho g V_w + \rho_c g V_c = 0, \qquad [21]$$

in which ρ_c represents the density of the core and V_c the volume of the core between x and $x + l$. Substitution of [9] and [14] in [21] then yields the following condition for steady core-annular flow

$$2R\int_0^{\pi}\int_0^{l} \phi\cos\theta\,d\theta\,dx - \int_0^{\pi}\int_0^{l} h\frac{\partial\phi}{\partial\theta}\sin\theta\,d\theta\,dx = (\rho - \rho_c)g V_c. \qquad [22]$$

At low water percentages $V_c \approx \pi R^2 l$ and [22] becomes

$$2R\int_0^{\pi}\int_0^{l} \phi\cos\theta\,d\theta\,dx - \int_0^{\pi}\int_0^{l} h\frac{\partial\phi}{\partial\theta}\sin\theta\,d\theta\,dx = (\rho - \rho_c)g\pi l R^2. \qquad [22']$$

Equation [22] states that in steady core-annular flow the buoyancy force on the core is counterbalanced by hydrodynamic lubrication forces.

For the horizontal direction ($i = 1$) [19] becomes, after substitution of σ'_{ij}

$$F_1 = \iint_{S_1} p\,dS - \iint_{S_2} p\,dS - 2\mu R\int_0^{\pi}\int_o^{l}\left(\frac{\partial w}{\partial y}\right)_{y=0} d\theta\,dx. \qquad [23]$$

As mentioned earlier, half-way between $x = 0$ and $x = nl\,p$ ceases to change over a wavelength, apart from the pressure drop due to the pressure gradient over the pipe. Hence

$$\iint_{S_1} p\,dS - \iint_{S_2} p\,dS = \frac{(\phi_1 - \phi_2)}{n} S_1. \qquad [24]$$

Substitution of [9], [15] and [24] in [23] yields

$$F_1 = \frac{(\phi_1 - \phi_2)}{n} S_1 + R\int_0^{\pi}\int_0^{l} h\frac{\partial\phi}{\partial x}\,d\theta\,dx + 2\mu R W\int_0^{\pi}\int_0^{l}\frac{1}{h}\,d\theta\,dx. \qquad [25]$$

The drag force F_1 on the core must be equal to the driving thrust on the core; thus

$$F_1 = \frac{(\phi_2 - \phi_1)}{n} S_5, \qquad [26]$$

in which, as shown in figure 3, S_5 is the surface area of a cross-section of the core. Substitution of [26] in [25] yields the following condition for core-annular flow

$$R \int_0^{\pi} \int_0^{l} h \frac{\partial \phi}{\partial x} \, d\theta \, dx + 2\mu RW \int_0^{\pi} \int_0^{l} \frac{1}{h} \, d\theta \, dx = \frac{\pi R^2 (\phi_2 - \phi_1)}{n}. \qquad [27]$$

4. SOLUTION PROCEDURE

Dimensionless axial distance $X = x/R$, annular thickness $H = h/R$, ripple length $L = l/R$, pressure $\Phi = \phi R/6\,\mu W$ and density $P = \rho R^2 g/6\,\mu W$ are introduced. Equation [8] becomes, in dimensionless form

$$\frac{\partial}{\partial \theta}\left(H^3 \frac{\partial \Phi}{\partial \theta}\right) + \frac{\partial}{\partial X}\left(H^3 \frac{\partial \Phi}{\partial X}\right) = \frac{\partial H}{\partial X}, \qquad [8']$$

while the boundary conditions become

$$\text{for } \theta = 0 : \frac{\partial \Phi}{\partial \theta} = 0 \qquad [10']$$

$$\text{for } \theta = \pi : \frac{\partial \Phi}{\partial \theta} = 0 \qquad [11']$$

$$\text{for } X = 0 : \Phi = \Phi_1 \qquad [12']$$

$$\text{for } X = nL : \Phi = \Phi_2. \qquad [13']$$

After introducing the dimensionless variables and dividing by πL condition [22'] can be written as

$$\frac{2}{\pi L} \int_0^{\pi} \int_0^{L} \Phi \cos\theta \, d\theta \, dX - \frac{1}{\pi L} \int_0^{\pi} \int_0^{L} H \frac{\partial \Phi}{\partial \theta} \sin\theta \, d\theta \, dX = P - P_c. \qquad [22']$$

Condition [27] becomes

$$\frac{1}{\pi L} \int_0^{\pi} \int_0^{L} H \frac{\partial \Phi}{\partial X} \, d\theta dX + \frac{1}{3\pi L} \int_0^{\pi} \int_0^{L} \frac{1}{H} \, d\theta \, dX = \frac{(\Phi_2 - \Phi_1)}{nL}. \qquad [27']$$

Originally the solution procedure was as follows. First $H(\theta, X)$ and a certain value for $(\Phi_2 - \Phi_1)$ were chosen. For H the sawtooth function of figure 2 defined by [1]–[4] was chosen. Then [8'] with the boundary conditions [10']–[13'] was solved. The calculated value of Φ was then substituted in [27') and it was usually found that this condition was not satisfied. So a new value for $(\Phi_2 - \Phi_1)$ was chosen and the calculation repeated; this iteration was continued until [27'] was satisfied. Substitution of the final solution for Φ in [22'] yielded the dimensionless density difference $(P - P_c)$ between annulus and core, which could be counterbalanced.

To avoid the iteration the following solution procedure was adopted. Without loss of generality take $\Phi_1 = 0$. Let $\Phi^{(u)}$ be the solution of [8'] and [10']–[13'], with $\Phi_2 = 1$ and the r.h.s. of [8'] being replaced by zero. Let $\Phi^{(c)}$ be the solution of [8'] and [10']–[13'] with $\Phi_2 = 0$. $\Phi = \Phi_2\Phi^{(u)} + \Phi^{(c)}$ is then the general solution. Let the first and second terms on the left of [27'] be called D_1 and D_2, i.e.

$$D_1 = \frac{1}{\pi L}\int_0^{\pi}\int_0^{L} H\,\frac{\partial \Phi}{\partial X}\,d\theta\,dX \qquad [28]$$

$$D_2 = \frac{1}{3\pi L}\int_0^{\pi}\int_0^{L} \frac{1}{H}\,d\theta\,dX. \qquad [29]$$

D_1 is linear in Φ and D_2 is independent of Φ. Let $D^{(c)} = D_1(\Phi^{(c)}) + D_2$. Then [27'] becomes

$$\frac{\Phi_2}{n}D_1(\Phi^{(u)}) + D^{(c)} = \frac{\Phi_2}{nL}. \qquad [30]$$

Hence the value of Φ_2 is given by

$$\Phi_2 = \frac{nD^{(c)}}{1/L - D_1(\Phi^{(u)})}. \qquad [31]$$

This solution procedure requires only two calculations; firstly for $\Phi^{(c)}$, from which $D^{(c)}$ is calculated, and secondly for $\Phi^{(u)}$, from which $D_1(\Phi^{(u)})$ follows. Φ_2 can be calculated from [31], after which the solution $\Phi = \Phi_2\Phi^{(u)} + \Phi^{(c)}$ is known. Substitution of this solution in [22'] yields the dimensionless density difference. The solution of [8'] with the boundary conditions [10']–[13'] has been performed with the aid of the finite element method.

5. FINITE ELEMENT METHOD

After multiplying [8'] by a variation $\delta\Phi(\theta, X)$ satisfying

$$\delta\Phi(\theta, 0) = 0 \text{ and } \delta\Phi(\theta, nL) = 0, \qquad [32]$$

and integrating over the domain Ω bounded by $X = 0$, $X = nL$, $\theta = 0$ and $\theta = \pi$ the following equation can be derived

$$-\iint_{\Omega} H^3\,\text{grad}\,\Phi \cdot \text{grad}\,\delta\Phi\,dS = \iint_{\Omega}\frac{\partial H}{\partial X}\,\delta\Phi\,dS. \qquad [33]$$

The derivation is standard and therefore omitted. It is noted that [10'] and [11'] are natural boundary conditions, so that only [12'] and [13'] are required to be imposed. Φ and $\delta\Phi$ are approximated by Φ^h and $\delta\Phi^h$ respectively, and Φ^h and $\delta\Phi^h$ have been taken as piecewise linear on a triangulation. After substitution of Φ^h and $\delta\Phi^h$ in [33] a linear system of equations is found, which can be solved. To save computer time the integrals occurring in these equations have been calculated using a three-point Gauss rule. An example of the mesh in the θ, X plane used in the calculation is given in figure 4. To investigate the numerical error in Φ, computations with one half of the grid size have been carried out.

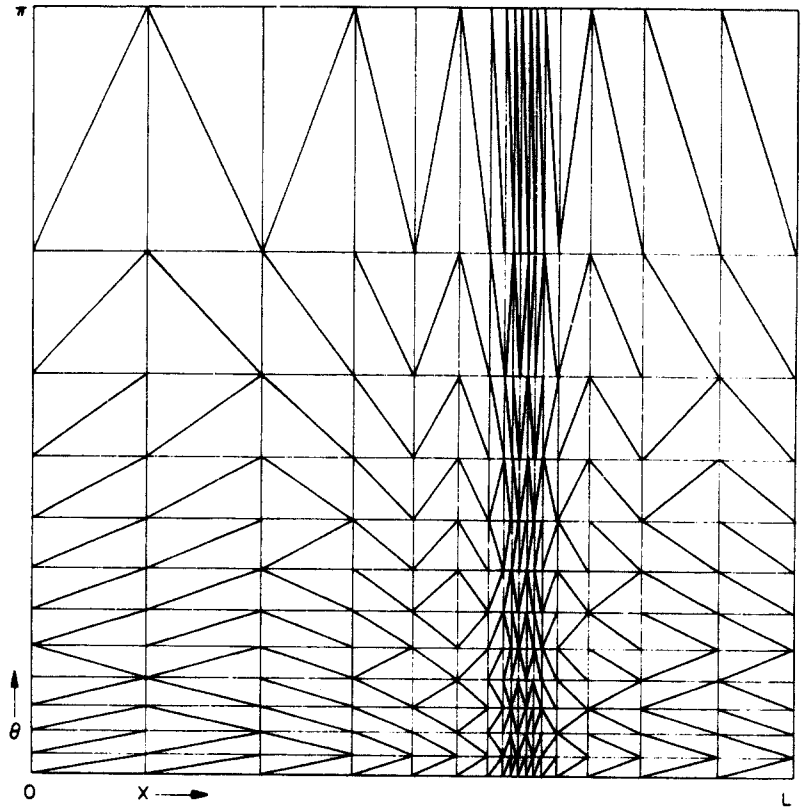

Figure 4. Example of mesh in θ, X plane used in the calculation.

6. RESULTS FROM THE THEORETICAL MODEL

The influence of the number of wavelengths n on the distribution of Φ in the water film was studied first. As mentioned earlier the objective in taking a number of wavelengths n into account is to find the periodic solution. To this end n was successively given the following values: 1, 7, 21 and 41. Equation [8'] with boundary conditions [10']–[13'] was solved for these values and the integrals of [22'] and [27'] calculated. For the water fraction ($\approx H_0 = h_0/R$), the dimensionless wavelength $L = l/R$, the dimensionless amplitude of the ripple $A = a/R$, the dimensionless location $L' = l'/l$ of the maximum of the ripple and the dimensionless eccentricity $E = e/R$ the following values were chosen: $H_0 = 0.06$, $L = 1$, $A = 0.006$, $L' = 0.9$ and $E = 0.053$. (As mentioned earlier the real core eccentricity is equal to $2e$; but in the following $E = e/R$ is called the dimensionless eccentricity, corresponding to the eccentricity at the top of the pipe, where the downthrust due to lubrication is greatest.) In this way it was investigated how many wavelengths were necessary for the Φ-distribution over a wavelength and for the integrals of [22'] and [27'] to become independent of the location in the pipe. In figure 5 the results are shown for the integral $(2/\pi L) \int_0^{\pi} \int_0^{L} \Phi \cos\theta \, d\theta \, dX$ from [22']. (The results for Φ and the other integrals are similar.) In this figure the value for the integral is given for each wavelength of the ripple; from the first between $X = 0$ and $X = L$ to the last between $X = (n-1)L$ and $X = nL$. After about three wavelengths the value of the integral is seen to become independent of the location of the wavelength. So $n = 7$ is sufficient for the lubrication approximation to settle to near-periodic conditions. To be on the safe side, $n = 13$ was used in all further calculations; the integrals of [22'] and [27'] were calculated from the Φ-distribution over the wavelength between $X = 6L$ and $X = 7L$.

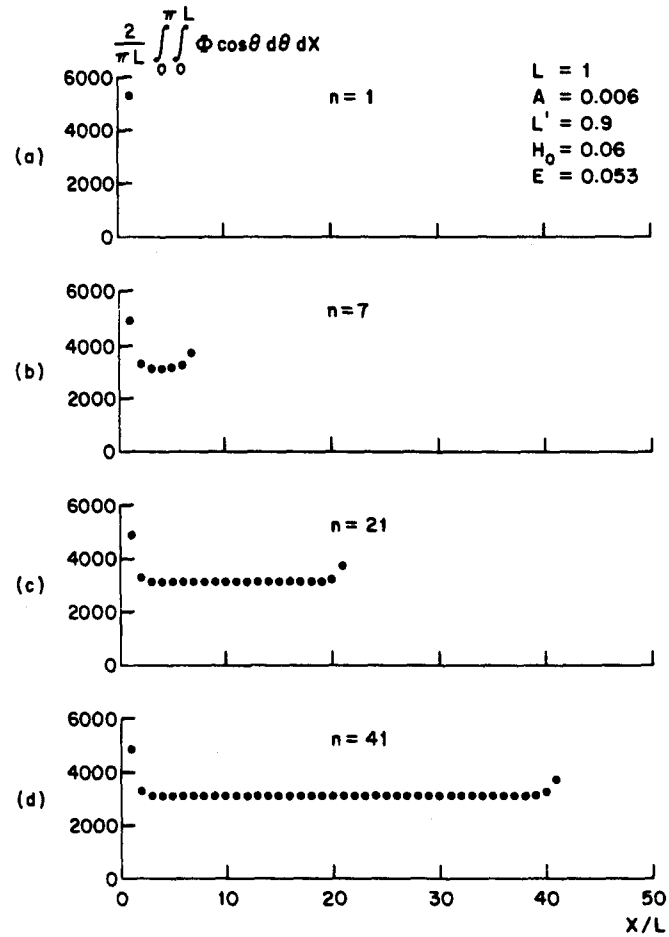

Figure 5. Distribution of $(2/\pi L)\int_0^{\pi}\int_0^{L}\Phi\cos\theta\,d\theta\,dX$ over a ripple of n wavelengths.

Next an initial calculation for core-annular flow was performed. For H_0, L, A and L' the following values were again chosen: $H_0 = 0.06$, $L = 1$, $A = 0.006$ and $L' = 0.9$. The dimensionless eccentricity $E = e/R$ was increased step by step from 0 to the value at which the core almost touches the pipe wall. For these values of the parameters, [8'] with the boundary conditions [10']–[13'] was solved and the integrals of [22'] and [27'] were calculated. Equation [22'] yields the dimensionless density difference $P - P_c$ between water and oil which can be counterbalanced by the lubrication forces. Equation [27'] gives the dimensionless pressure gradient over the pipe. The results are shown in figures 6(a) and (b). The dots in these figures are the calculated points. The point where the core touches the pipe wall is indicated in the figures. In figure 6(a) the density difference required † for steady core-annular flow in the case of $\rho - \rho_c = 100\ \text{kg/m}^3$, $\mu = 1$ mPa.s,‡ $W = 0.2$ m/s and $R = 0.025$ m is also given. The value of E at which the dimensionless density difference which can be counterbalanced is equal to the required dimensionless density difference gives the dimensionless eccentricity at which steady core-annular flow is possible.

From figure 6(b) the dimensionless pressure gradient for steady core-annular flow can then be found. As can be seen from figure 6(a), steady core-annular flow is only possible with a very

†i.e. required for a balance between the lubricaton force and buoyancy force.
‡1 mPa.s = 0.001 kg/ms.

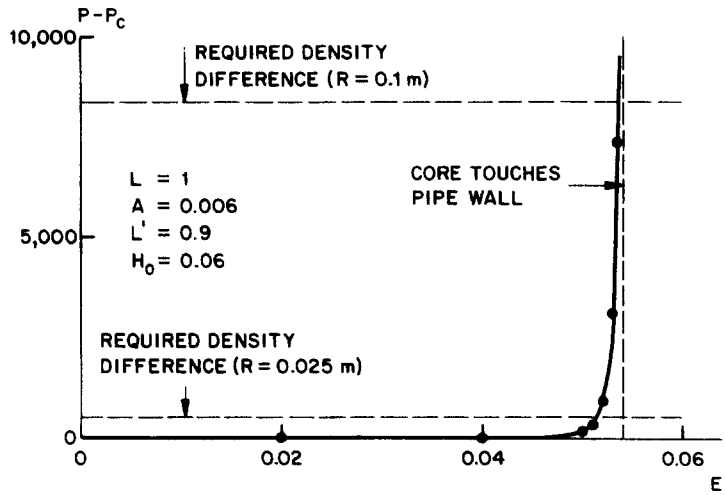

Figure 6(a). Dimensionless density difference as a function of the dimensionless eccentricity.

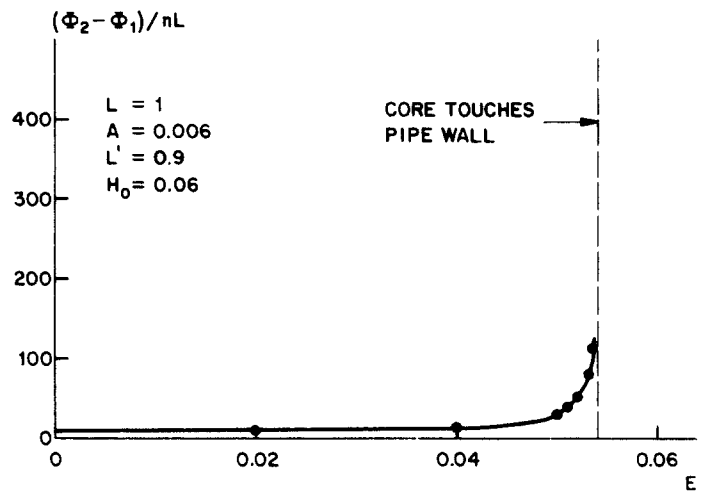

Figure 6(b). Dimensionless pressure gradient as a function of the dimensionless eccentricity.

eccentric core. Only when the annular film in the upper part of the pipe has become very thin are the lubrication forces large enough to counterbalance the buoyancy force of the core.

In figure 6(a) the dimensionless density difference required for steady core-annular flow in an 8-inch pipe ($R = 0.1$ m) with $\rho - \rho_c = 100$ kg/m^3, $\mu = 1$ mPa.s, and $W = 0.2$ m/s is also given. From figure 6(a) it can be concluded that, for steady core-annular flow in an 8-inch pipe ($R = 0.1$ m), greater dimensionless eccentricity is required than in a 2-inch pipe ($R = 0.025$ m). From figure 6(b) it then follows that the dimensionless pressure gradient is also larger. So the dimensionless pressure gradient increases with the pipe diameter.

In figure 7 the distribution of $\Phi^{(c)}$ over the wavelength between $X = 6L$ and $X = 7L$ for five values of θ is given for $H_0 = 0.06$, $L = 1$, $L' = 0.9$, $A = 0.006$ and $E = 0.053$. As can be seen, the variations in $\Phi^{(c)}$ (and thus in the pressure p) are very large only in the upper part of the pipe, where the water film is very thin. In the lower part of the pipe the variations are negligibly small.

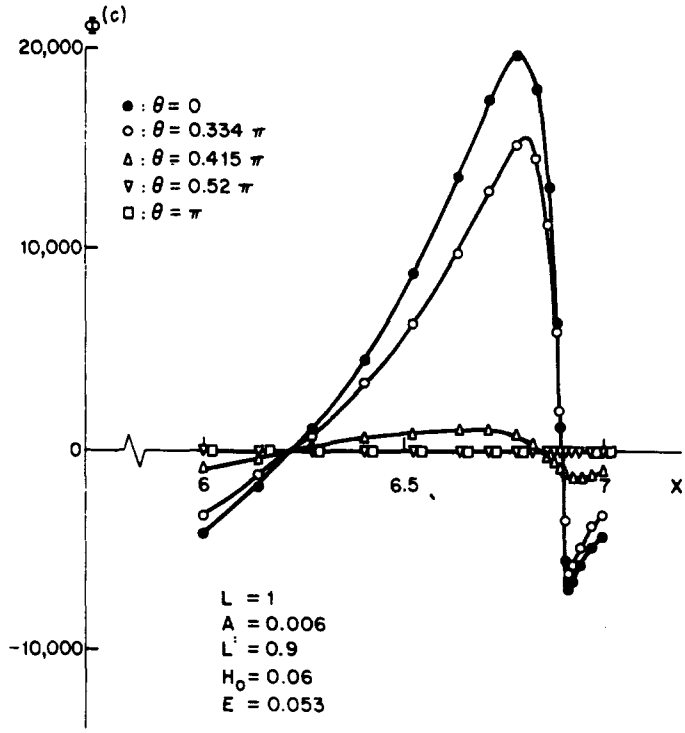

Figure. 7. Pressure, $\Phi^{(c)}$, distribution over a wavelength of the ripple for five different radial positions of θ.

The azimuthal film flow can be understood by substitution of the results for $\Phi^{(c)}$ from figure 7 in [14]. On one side of the ripple the pressure is higher at the top than at the bottom. The pressure gradient drives the water out of the thin upper film around the core to the thick lower film. However, at the other side of the ripple the pressure at the top is lower than at the bottom. By this reverse pressure gradient the water is driven back to the upper film. So superimposed on the flow in the axial direction of the pipe there is an oscillatory azimuthal film flow; the azimuthal flow changes direction from one side to the ripple to the other side.

It is difficult to measure accurately the ripple parameters, such as wavelength and amplitude, from the observations. Therefore, a sensitivity study has been carried out to investigate the influence of these parameters on the hydrodynamic lubrication of the core by the water film. The influences of the dimensionless wavelength L, the dimensionless amplitude A, the dimensionless location L' of the maximum of the ripple amplitude and the water fraction ($\approx H_0 = h_0/R$) have been studied. As a reference case the following values were selected: $L = 1$, $A = 0.003$, $L' = 0.9$ and $H_0 = 0.02$. One of the parameters was varied, while the others were kept constant.

Figures 8(a) and (b) present the results for L. Figure 8(a) shows the dimensionless density difference $P - P_c$, which can be counterbalanced by the lubrication force, as a function of the dimensionless eccentricity E for three values of L. Again, the values of the dimensionless density difference which are required for steady core-annular flow with $\rho - \rho_c = 100\ \mathrm{kg/m^3}$, $\mu = 1$ mPa.s, $W = 0.2$ m/s and $R = 0.025$ m or $R = 0.1$ m are also indicated in the figure, as is the eccentricity where the core touches the pipe wall. Figure 8(b) shows the dimensionless pressure gradient $(\Phi_2 - \Phi_1)/nL$ over the pipe as a function of E for the three values of L. From the figures it can be concluded that, when L decreases, the eccentricity where the dimensionless density difference is equal to the required dimensionless density difference increases, and the dimensionless pressure gradient increases. However, the effect is not very strong in the region of parameter values where the calculations were performed.

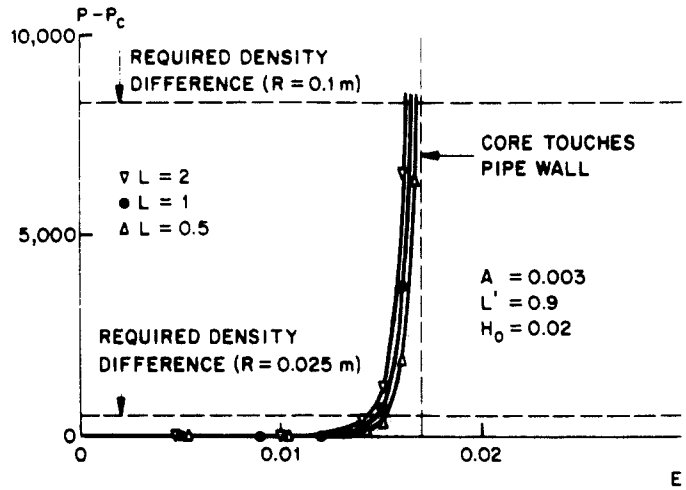

Figure 8(a). Dimensionless density difference as a function of dimensionless eccentricity for three values of L.

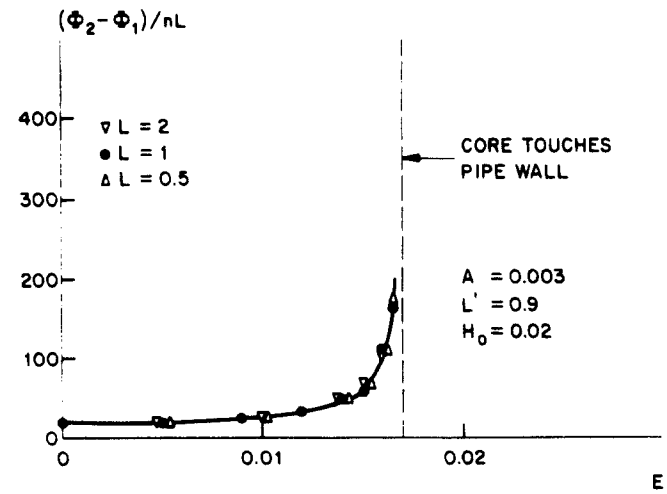

Figure 8(b). Dimensionless pressure gradient as a function of dimensionless eccentricity for three values of L.

Figures 9(a) and (b) present the results for A. When A decreases, the eccentricity at which the dimensionless density difference is equal to the required value increases, and the dimensionless pressure gradient increases. When the ripple decreases completely ($A = 0$), the eccentricity increases until the core touches the upper part of the pipe wall. In this case the dimensionless pressure gradient becomes very large.

Figures 10(a) and (b) present the results for L'. When L' decreases, the eccentricity where the dimensionless density difference is equal to the required value increases, and the dimensionless pressure gradient increases. When the ripple is symmetrical ($L' = 0.5$) the eccentricity increases until the core touches the pipe wall. In such a case the dimensionless pressure gradient again becomes very large.

Figure 11(a) and (b) give the results for different values of H_0. When H_0 decreases, the eccentricity where the dimensionless density difference is equal to the required value decreases, and the dimensionless pressure gradient increases. The thickness of the water film in the upper part of the pipe increases only slightly. When more water is supplied, the greater portion of it

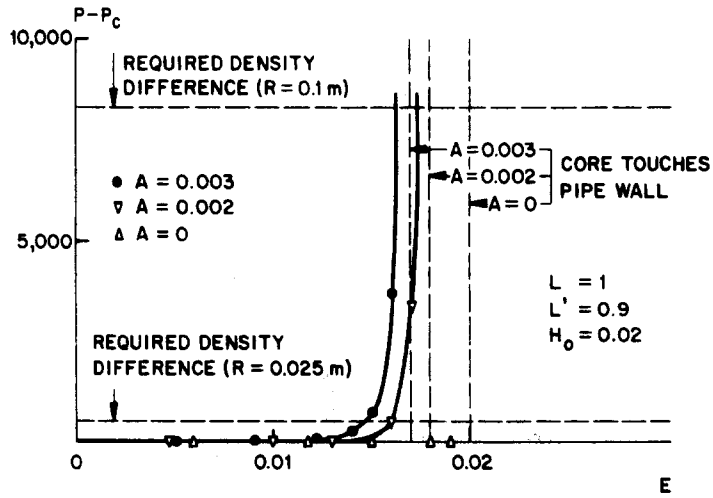

Figure 9(a). Dimensionless density difference as a function of dimensionless eccentricity for three values of A.

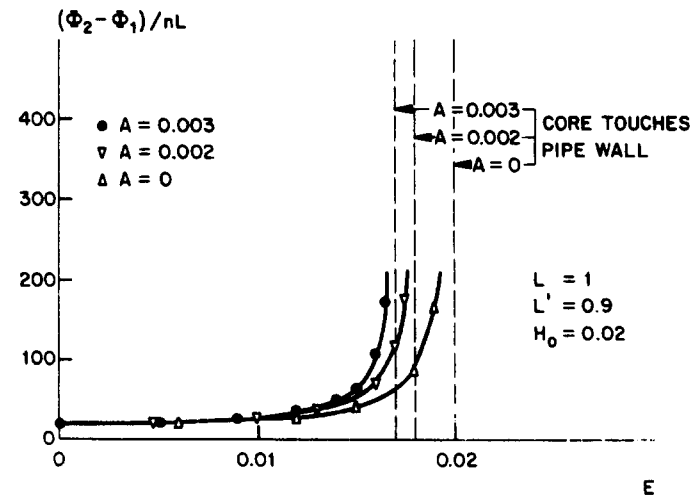

Figure 9(b). Dimensionless pressure gradient as a function of dimensionless eccentricity for three values of A.

goes to the lower part of the pipe. This is qualitatively similar to the visual observations represented in figure 1.

7. EXPERIMENTS IN A 2-INCH AND AN 8-INCH PIPELINE

In order to investigate whether, with the theoretical model, realistic pressure gradient predictions can be made for core-annular flow in larger pipes, a base set of reliable experimental data is required. To this end, experiments were carried out with high-viscosity oil (500 mPa.s† and more) in a number of pipes with sizes ranging from 1 to 8 inches. Here we present some of the results for a 2-inch and an 8-inch pipe.

The first set of experiments was performed in the 2-inch pipe described in section 2. The difference in density between water and oil was about 30 kg/m^3. The amount of water was varied between 20 and 3%. The oil viscosities varied from 2300 to 3300 mPa.s.

†1 mPa.s = 1 cP.

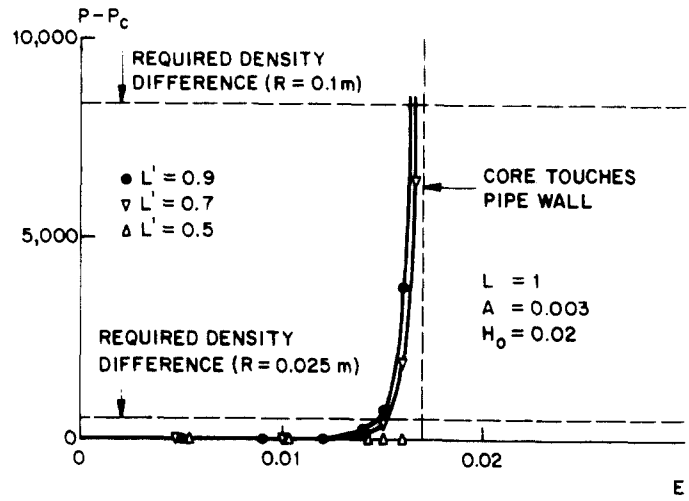

Figure 10(a). Dimensionless density difference as a function of dimensionless eccentricity for three values of L'.

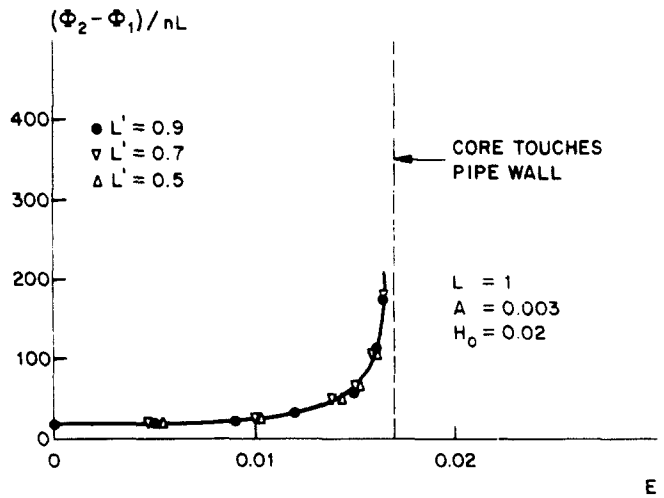

Figure 10(b). Dimensionless pressure gradient as a function of dimensionless eccentricity for three values of L'.

The second set of experiments was carried out in horizontal 8-inch pipe circuit, 888 m long, comprising 22 right-angle bends of 2.5–1.5 D radius, which did not pose any problems for stable core-annular flow operation. The difference in density between water and oil was about 45 kg/m^3. The oil viscosities for the pressure gradient tests considered here varied from 1200 to 2200 mPa.s, at a superficial oil velocity of 1 m/s. In these tests the input water fraction ranged from 10% to 1%.

The pressure gradient ratios ($\Delta P_{ow}/\Delta p_{so}$) measured in the 2-inch and 8-inch pipes at a superficial velocity of approximately 1 m/s are summarized in figure 12. Δp_{ow} represents the pressure drop over the pipe for core-annular flow. Δp_{so} is the pressure drop when only oil flows through the pipe at the same superficial oil velocity as for core-annular flow. It is quite remarkable that, when the percentage of water is so small, the pressure gradient ratio hardly changes with water fraction. It is also evident that for the larger pipe the benefit of core-annular flow operation is smaller than for the 2-inch pipe: the average pressure loss ratio is

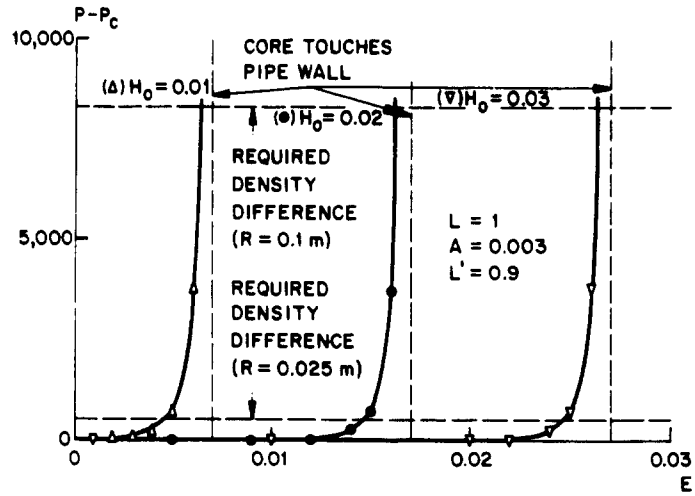

Figure 11(a). Dimensionless density difference as a function of dimensionless eccentricity for three values of H_0.

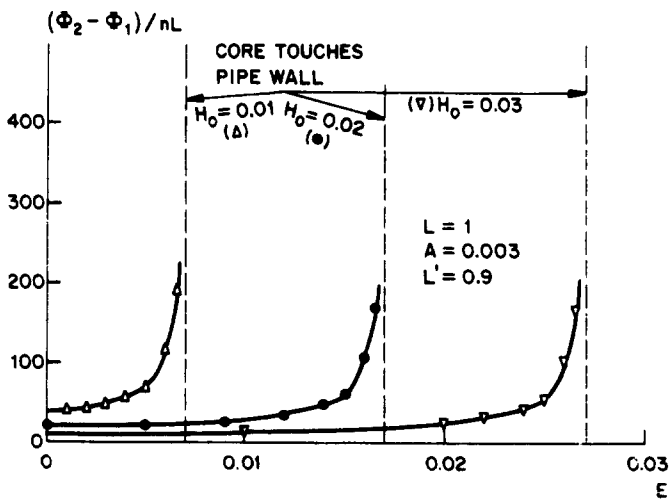

Figure 11(b). Dimensionless pressure gradient as a function of dimensionless eccentricity for three values of H_0.

0.10 as against 0.01 for the 2-inch pipe. In figure 12 V_{so} represents the superficial oil velocity, μ_0 the oil viscosity and $\Delta\rho = \rho - \rho_c$.

8. COMPARISON BETWEEN THEORETICAL MODEL AND EXPERIMENTS

For known interfacial wave characteristics (the parameters A, L and L') and for a known dimensionless thickness of the water annulus H_0, calculations with the theoretical model for a particular pipe size are performed as follows:

—plots are determined for the dimensionless density difference, $P - P_c$, and the dimensionless pressure gradient per unit length, $(\Phi_2 - \Phi_1)/nL$, as a function of core eccentricity, E (e.g. as shown in figure 6);

—the eccentricity is found which corresponds to the dimensionless density difference for the particular pipe problem;

—with this eccentricity, the dimensionless pressure gradient is calculated.

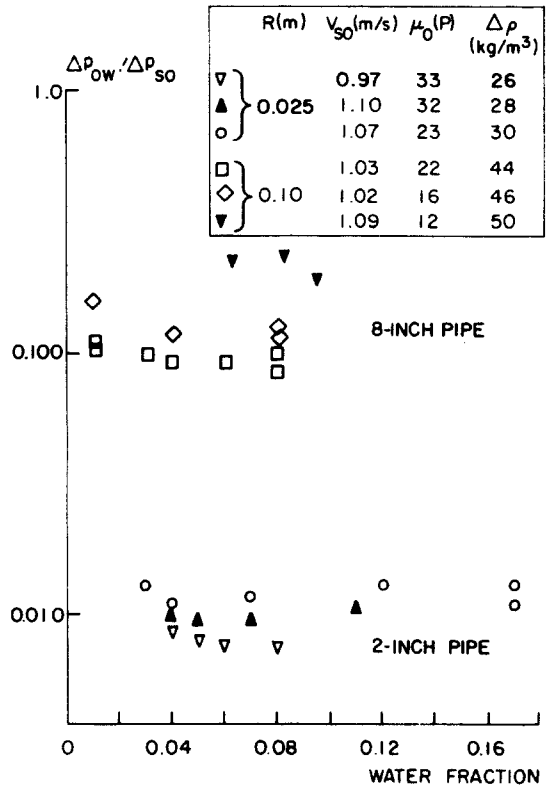

Figure 12. Pressure gradient ratios measured in a 2-inch and an 8-inch pipe for various input water fractions.

The main problem is what values to choose for the parameters that describe the interfacial wave. We took as a basis the photographs taken during the tests in the 2-inch pipe (see figure 1) and the pressure losses measured. For tests with water fraction of 0.06 our best estimates for these parameters are $A = 0.003$, $L = 0.8$, $L' = 0.8$ (L and L' were determined from the photographs, while the value chosen for A is the one that gives best agreement with the pressure loss measured). This choice corresponds to an average wave amplitude of 0.075 mm and a wavelength of 20 mm, i.e. nearly equal to the pipe radius. With regard to the 8-inch pipe, no information on wave characteristics is available; however, since the tests in this larger pipe were performed with similar crude oils, we used the same absolute values for the wave parameters. The dimensionless parameters A and L, being inversely proportional to R, are then smaller than for the 2-inch pipe. This guarantees, as can easily be verified, that, for a core velocity of 1 m/s, all three conditions [5], [6] and [7] for the applicability of the lubrication theory are satisfied in the upper part of the pipe for all pipe sizes of 2 inches and larger. At the bottom, condition [7] is in general not satisfied. However, as has been shown, the important part of the water film is at the top, where the downthrust due to lubrication forces is generated. The lubrication forces at the bottom are neglegible. Moreover, when we consider larger core velocities with less eccentricity, a point will be reached (at some critical velocity, which will depend on the individual pipe size) when condition [7] is no longer satisfied at the top, either.

In figure 13 we have plotted pressure gradient ratios measured in the 2-inch pipe with average oil viscosities of 2300, 3200 and 3300 mPa.s and superficial oil velocities of about 1 m/s, and results of calculations with the theoretical model. The measured data scatter around the calculated values; the average deviations do not exceed 7%.

The theoretical model will only be a valuable tool in the designing of pipelines for core-annular flow operation if it can be scaled up to larger pipe sizes. A check for the ability of

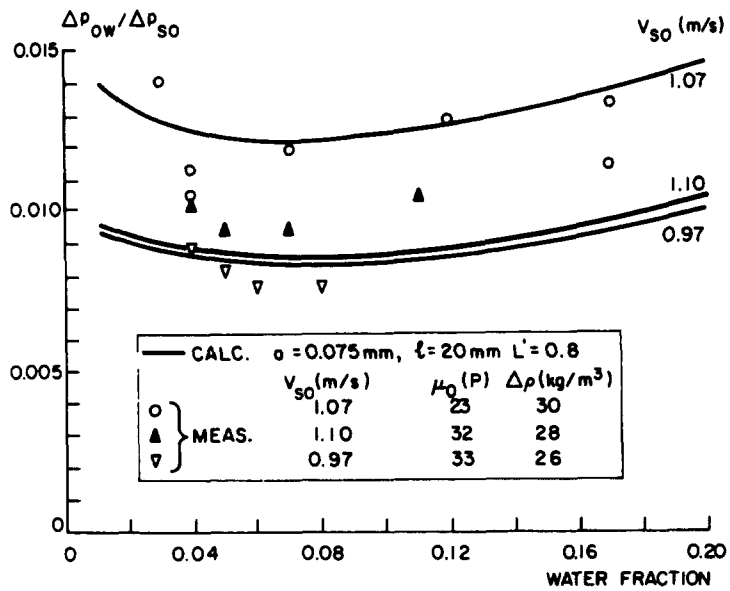

Figure 13. Measured and calculated pressure loss ratios for core-annular flow in a 2-inch pipe.

the model to make reasonable predictions, using the estimated parameter values for the interfacial waves, for pipe sizes other than 2 inches is a crucial test. We put our model to this test with a calculation for the 8-inch pipe. We used a water fraction of 0.06 as a typical case. Figure 14 shows measured and calculated pressure loss ratios for six test series, three in the 2-inch pipe and three in the 8-inch pipe. Model predictions for the 8-inch pipe are promising, although there is a systematic deviation of some 30%. The operating conditions under which the measurements given in figure 14 were obtained can be found in figures 12 and 13.

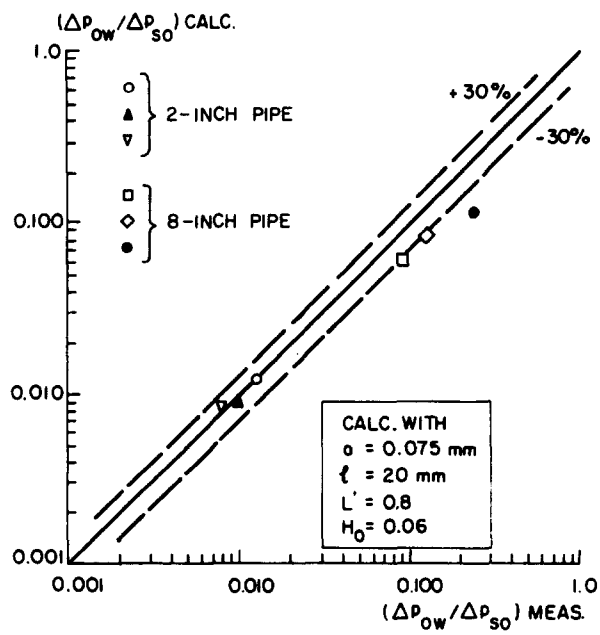

Figure 14. Measured and calculated pressure loss ratios in a 2-inch and an 8-inch pipe.

9. CONCLUDING REMARKS

A theoretical model for oil–water core-annular flow through a pipe has been developed. According to this model the movement of the rippled oil core with respect to the pipe wall induces pressure variations in the water film, which can exert a force on the core in a vertical direction. This force can be so great that it counterbalances the buoyancy force on the core, allowing a steady core-annular flow to arise.

The ripples in the core are essential: if the amplitude of the ripple becomes zero, there will no longer be a force on the core to counteract the buoyancy force. In such a case the core will rise in the pipe, until it touches the pipe wall.

The magnitude of the force also depends to a large extent on the shape of the ripple; when the ripple is symmetrical, again, no counteracting force will be present.

Adding more water to the flow does not change the flow pattern very much. The additional water largely goes to the lower part of the pipe. This is in agreement with observations.

To check the validity of the model, oil-water core-annular flow experiments have been carried out in a 2-inch and in an 8-inch pipe. These experiments indicate that core-annular flow becomes less advantageous for larger pipe sizes. This is correctly predicted by the model, although pressure loss ratios computed for the 8-inch pipe are some 30% too low. This could be due to turbulence in the lower part of the water film, which could become increasingly important for larger pipe sizes. This is a point of further study.

For reliable application of the model more knowledge is required about the amplitude and wavelength of the interfacial waves and about the thickness of the water film in the upper part of the pipe as a function of the flow parameters. Work to this end is in hand.

Acknowledgement—The authors are indebted to Dr. A. K. Chesters of Delft University of Technology for stimulating discussions.

REFERENCES

CHARLES, M. E. GOVIER, G. W. & HODGSON, G. W. 1961 The horizontal pipeline flow of equal density oil–water mixtures. *Can. J. Chem. Engng* **39**, 27–36.

TIPEI, N. 1962 *Theory of Lubrication.* Stanford University Press.

YIH, C. S. 1967 Instability due to viscosity stratification. *J. Fluid Mech.* **27**, 337–352.